Improved light extraction of organic light emitting diodes with a nanopillar pattering structure*

Gao Zhi-Xiang(高志翔)[a)b)], Wang Hua(王 华)[a)c)], Hao Yu-Ying(郝玉英)[a)d)], Miao Yan-Qin(苗艳勤)[a)c)], and Xu Bing-She(许并社)[a)c)†]

[a)] *Key Laboratory of Interface Science and Engineering in Advanced Materials of Ministry of Education, Taiyuan University of Technology, Taiyuan* 030024, *China*

[b)] *School of Physical Science and Electronics, Shanxi Datong University, Datong* 037009, *China*

[c)] *Research Center of Advanced Materials Science and Technology, Taiyuan University of Technology, Taiyuan* 030024, *China*

[d)] *Department of Physics and Optoelectronics, Taiyuan University of Technology, Taiyuan* 030024, *China*

(Received 27 March 2013; revised manuscript received 14 May 2013)

We have investigated the properties of organic light emitting diodes (OLEDs) with a nanopillar patterning structure at organic–metal or organic–organic interfaces. The results demonstrate that the introduction of a nanopillar structure can improve the light extraction efficiency greatly. We also find that the number, height, and position of nanopillars all affect the light extraction of OLEDs. The maximum power efficiency of a device with an optimized nanopillar patterning mode can be improved to 2.47 times that of the reference device. This enhancement in light extraction originates from the improved injected carriers, the broadened charge recombination zone, and the intensified wave guiding effects.

Keywords: organic light-emitting diodes, nanopillar, current efficiency, light extraction

PACS: 68.35.−p, 85.35.−p, 78.55.Kz **DOI:** 10.1088/1674-1056/22/11/116801

1. Introduction

Organic light-emitting diodes (OLEDs) have attracted considerable attention due to their potential commercial applications in flat panel displays and large-area solid-state illumination light sources, owing to advantages of low drive voltage, high luminance, easy manufacturability, and large-area extendibility.[1–6] However, the performance of OLEDs needs to be improved for future wide utilization, and much effort has been made.[7–12] Among these efforts, improving the luminous efficiency of OLEDs has been a key issue that must be solved for their applications in lighting and displays.

Generally, only a small fraction of the total photons generated inside OLED thin films is utilized, owing to wave guiding effects and total internal high reflection coefficient in nanofilms. The light extraction efficiency of OLEDs is usually below $\sim 20\%$ of the internal efficiency,[13] which needs to be increased. Plenty of work related to light extraction schemes has been reported.[14–17] For example, random textures or ordered microcavity arrays have been employed on the top surface of the glass substrate to minimize the total internal reflection.[18–21] Recently, the introduction of a nanopillar structure into the OLED was proposed and implemented successfully.[22–24] Prompted by those studies on nanopillar structure OLEDs, we have devoted considerable effort to applying a similar approach to OLEDs.

In this study, we introduce a novel OLED with a nanopillar patterning structure, which exhibits high light extraction efficiency. Moreover, we have investigated the effects of the nanopillar position, nanopillar number, and height on the light extraction of OLEDs.

2. Experimental details

The devices were fabricated in a vacuum deposition instrument in our laboratory. Prior to organic layer deposition, indium-tin-oxide (ITO) glasses (sheet resistance of about 10 $\Omega/\square$) were cleaned successively by deionized water and acetone in an ultrasonic bath, dried in a drying cabinet, and exposed to a UV-ozone environment for 15 min. All organic layers were grown under thermal evaporation at the base pressure of $\leq 5 \times 10^{-4}$ Pa. The typical deposition rates were 0.6 Å/s, 0.1 Å/s, and 5.0 Å/s for organic materials, lithium fluoride (LiF), and aluminum (Al), respectively.

The active area of devices is 2.0×2.0 mm^2, in which a third of the nanopillars with width of 0.5 mm were implanted, as shown in Fig. 1(a). The cleaned substrates were put in the pallet of a deposition chamber (Fig. 1(b)). Then, the pallet was transferred into a vacuum chamber, and the shadow mask with a rectanglular frame was opened for sequential deposition of all organic functional layers. In the case of depositing nanopillar patterning, the pallet was transferred onto the

*Project supported by the Program for Changjiang Scholar and Innovation Research Team in Universities of China (Grant No. IRT0972), the International Science & Technology Cooperation Program of China (Grant No. 2012DFR50460), the National Natural Scientific Foundation of China (Grant Nos. 21071108, 60976018, 21101111, 61274056, and 61205179), and the Key Innovative Research Team in Science and Technology of Shangxi Province, China (Grant No. 2012041011).

†Corresponding author. E-mail: xubs@tyut.edu.cn

© 2013 Chinese Physical Society and IOP Publishing Ltd

shadow mask with 1–3 line arrays. Finally, the Al cathode was deposited onto organic layers by using a metal shadow mask. The nanopillar array was located in the center of the active area. The masks for depositing organic layers, nanopillars, and the Al cathode are shown in Fig. 1(c).

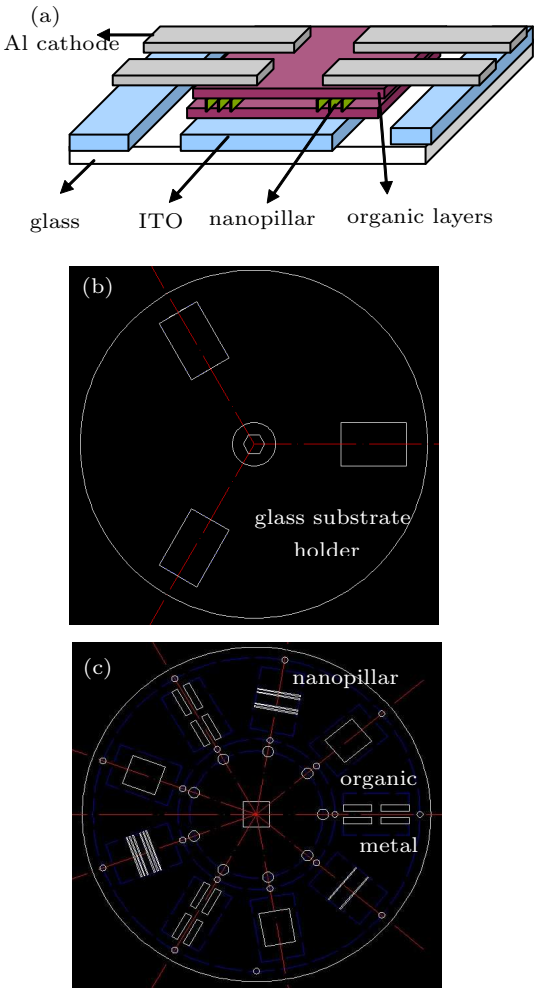


Fig. 1. (color online) Fabrication process of nanopillar-pattern OLEDs. (a) Schematic diagram of the OLEDs fabricated in this work; (b) substrate pallet; (c) shadow mask for depositing organic layers, nanopillar pattern, and Al cathode.

The thickness of the films and the nanopillar height were controlled by a quartz thickness monitor and a Dektak XT surface profilometer. The structure of the devices and the chemical structures of the organic materials involved in this work are shown in Fig. 2(a): N,N′-bis-(naphthyl)-N,N′-diphenyl-1,1′-biphenyl-4,4′-diamine (NPB) was used as the hole transport layer (HTL), a tris(8-hydroxyquinoline)aluminum (Alq_3) layer was employed as an electron injection layer (EIL), the 1,3,5-tris(N-phenylbenzimidazol-2-yl)benzene (TPBi) was used as an electron transport layer (ETL), $Ir(ppy)_3$ (5 wt%) dopant in the host material of CBP was used as a light emitting layer, and a LiF/Al layer was used as a cathode.

First, we have fabricated one set of devices with the structure of ITO/NPB (30 nm)/CBP:$Ir(ppy)_3$(30 nm, 5%)/TPBi (10 nm)/Alq_3 (25 nm)/Alq_3 (5 nm) (n nanopillars)/LiF(1 nm)/Al(200 nm). Here, n was the number of patterned nanopillars in the Alq_3 layer adjacent to the cathode, which was set to be 0, 1, 2, and 3 for Devices A0, A1, A2, and A3, respectively.

As shown in Fig. 2(b), we have investigated the second set of devices with the structure of ITO/NPB (30 nm)/CBP:$Ir(ppy)_3$(30 nm, 5 %)/TPBi (10 nm)/Alq_3 (30 − x nm)/Alq_3 (x nm) (2 nanopillars)/LiF(1 nm)/Al(200 nm). Here, the variable x represents the thickness of the nanopillar filled with Alq_3, which was set to be 0, 5, 10, 15, and 20 nm for Devices A0, A2, B2, C2, and D2, respectively.

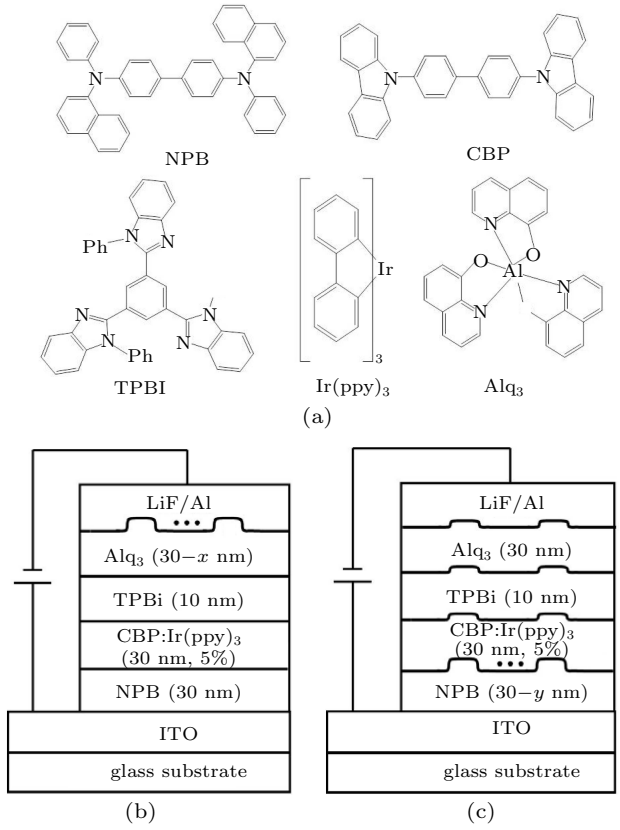


Fig. 2. Organic materials and device structure. (a) Chemical structures of the organic compounds used in this work; (b) devices with a nanopillar pattern structure at the ETL layer/cathode interface; (c) devices with a nanopillar pattern structure at the HTL/EML interface.

To further verify the effect of the location of the nanopillars in an OLED, we studied a third set of devices with the structure of ITO/NPB (30-y nm)/NPB (y nm) (2 nanopillars)/CBP:$Ir(ppy)_3$(30 nm, 5%)/TPBi (10 nm)/Alq_3(30 nm)/LiF(1 nm)/Al(200 nm) (Fig. 2(c)). Here, the variable y was 5, 10, 15, and 20 nm for Devices E2, F2, G2, and H2, respectively.

The current density–voltage–luminance (J–V–L) and electroluminescence (EL) spectra of OLEDs were measured simultaneously by using a testing setup comprising of a Keithley 2400 Source Meter and a Spectra Scan PR655 (Photo Research Inc.). All measurements were carried out at room

temperature under ambient conditions. The layer setup and maximum current efficiency of each device are summarized in Table 1.

Table 1. The performance of devices with different nanopillar patterning modes.

Nanopillar patterning	Symbol Symbol	Number of nanopillar	Height of nanopillar/nm	Maximum current efficiency/cd·A^{-1}
Reference	A0	0	0	15.17
ETL/Cathode interface	A1	1	5	15.79
	A2	2	5	20.95
	A3	3	5	18.60
	B2	2	10	22.84
	C2	2	15	21.13
	D2	2	20	19.49
HTL/EML interface	E2	2	5	23.06
	F2	2	10	25.51
	G2	2	15	27.05
	H2	2	20	20.99

3. Results and discussion

3.1. Effect of nanopillar number at the Alq_3/LiF interface

The electroluminescent characteristics of Devices A0, A1, A2, and A3 are shown in Fig. 3. It can be seen that the current density under voltage above 6.0 V of Devices A1, A2, and A3 was higher than that of the reference device (Device A0), owing to variations in the distribution of electric field and carrier accumulation located at the interface area between adjacent organic layers originated from nanopillar-pattern interfaces in Devices A1, A2, and A3. For the voltage above 7 V, it is clearly observed that the *L*–*V* and *J*–*V* curves for Devices A1, A2, and A3 are higher than that for Device A0. Moreover, it is found that Device A2 exhibits the highest current efficiency of 20.95 cd/A and power efficiency of 8.56 lm/W among nanopillar-pattered devices, which was nearly 1.38 and 1.62 times that of Device A0, respectively (Figs. 3(c) and 3(d)). The remarkably improved efficiency of Devices A1–A3 is attributed to the improvement in the light extraction efficiency of the above OLEDs, as illustrated in Fig. 4. Compared with the reference device (Fig. 4(a)), the device with a nanopillar pattern (Fig. 4(b)) will reduce an edge light-emission mode and intensify light out-coupling into an external mode. This phenomenon is similar to the improved light out-coupling effect using a microcavity-patterned substrate.[22–24]

When the number of nanopillars in Alq_3 film adjacent to the cathode is increased to 3 (Device A3), the current efficiency and power efficiency began to drop. When the number of nanopillars is increased, the gap between nanopillars decreases, resulting in an improvement in the relative ratio of nanopillar height to the gap distance. Therefore, the electric field-induced transporting carriers are confined at the interface of the EML/cathode and form a phosphorescence quenching center, lower current, and power efficiency.

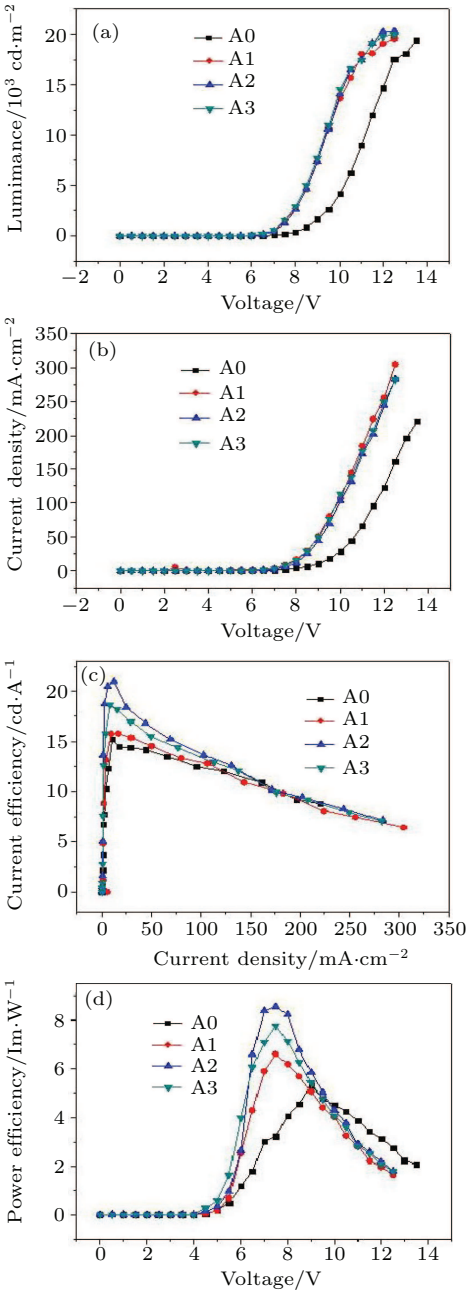


Fig. 3. (color online) The electroluminescent (EL) characteristics of devices A0, A1, A2, and A3, respectively. (a) Luminance-voltage characteristics; (b) current density-voltage curves; (c) current efficiency-current density curves; (d) power efficiency-voltage curves.

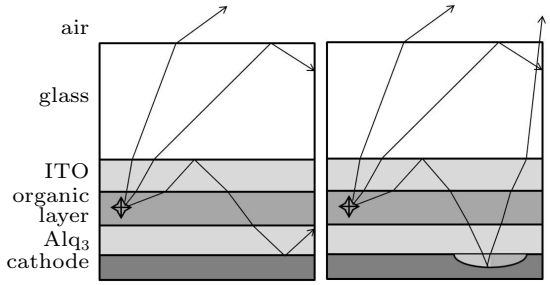


Fig. 4. The light out-coupling path for (a) the reference device and (b) nanopillar patterning device.

3.2. Effect of the nanopillar height at the Alq3/LiF interface

We change the nanopillar height for the devices with two nanopillars, in which the thickness of the total Alq_3 layer was 30 nm. Figure 5 shows the maximum current efficiency of devices with different heights of nanopillars (i.e., Device A2, B2, C2, and D2) and the Device A0. Results clearly indicate that Device B2 with a nanopillar height of 10 nm exhibits the maximum efficiency of 22.84 cd/A, which is about 1.51 times that of Device A0.

Then, we observe the nanopillar microstructure in Device B2 by using a crystalline phase microscope and surface profilometry. As shown in Fig. 6, the width and height of nanopillars in Device B2 were nearly 0.5 mm and 10 nm, respectively.

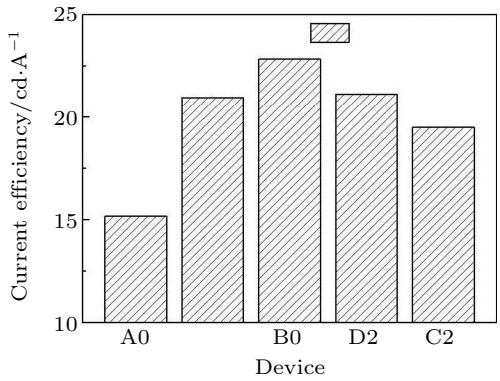


Fig. 5. The maximum current efficiency of devices with different heights of nanopillars at the Alq3/LiF interface layer (5 nm, 10 nm, 15 nm, and 20 nm) and the reference device.

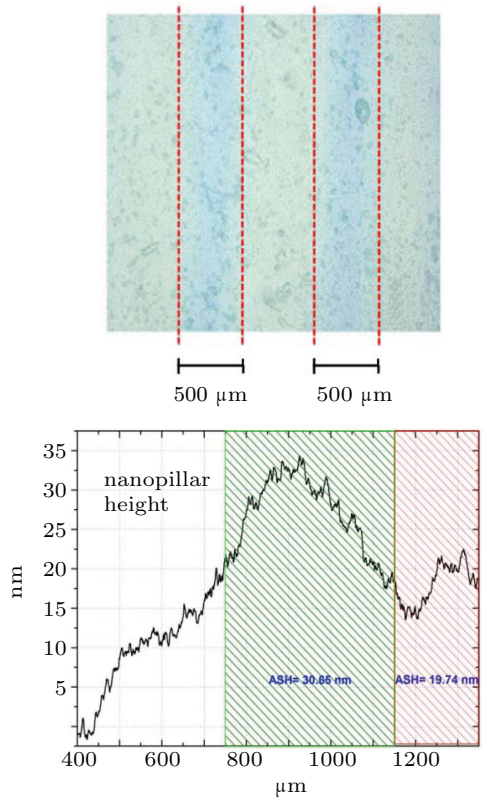


Fig. 6. (color online) The interface profile of nanopillars. Microstructure in Device B2 observed by (a) a crystalline phase microscope and (b) surface profilometry.

The change in nanopillar height can vary the total internal reflection at the Alq_3/LiF interface and the distribution of balanced hole-electron pairs, and affect light extraction eventually. The higher efficiency in Device B2 than that in Devices A2, C2, and D2 is due to a promotion in the escape of photons trapped in organic–organic modes and high index guided modes.[25,26]

3.3. Effect of the nanopillar position at difference interfaces

When nanopillars are located at the HTL/EML interface (Fig. 1(c)), it is found that the power efficiency is further strengthened relative to Device B2, which possesses the best performance among all OLEDs with a nanopillar located at the ETL/cathode interface (Fig. 7). In the case of a patterning structure with two nanopillars at the NPB/CBP:Ir(ppy)$_3$ interface, the current efficiency of Device G2 with a nanopillar height of 15 nm is higher than that of Devices E2, F2, and H2, as shown in the inset of Fig. 7. Device G2 is found to achieve a maximum current efficiency of 27.05 cd/A and a power efficiency of 13.06 lm/W, which is about 1.78 and 2.47 times that of the Device A0, respectively.

The remarkable improvement in power efficiency of Device G2 is contributed by several factors. First, it is considered that the nanopillar patterning structure at the NPB/CBP:Ir(ppy)$_3$ interface can increase the contact area and improve the injected carrier concentration at the NPB/CBP:Ir(ppy)$_3$ interface. Next, the nanopillar patterning interface will broaden the carrier recombination space because a majority of the carrier recombination occurs at the area adjacent to the NPB/CBP:Ir(ppy)$_3$ interface (Fig. 8), which avoids carrier accumulation and reduces the triplet–triplet (T–T) annihilation. Finally, the light extraction of the device is intensified by the efficient waveguide mode and surface plasmon mode originating from the NPB/CBP:Ir(ppy)$_3$ interface with a nanopillar patterning structure.

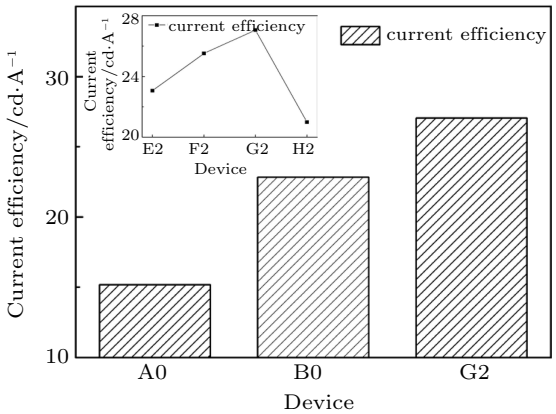


Fig. 7. The maximum current efficiency of devices with two nanopillars located at the HTL/EML interface and the reference device. The inset shows the maximum current efficiency of all devices with a third of nanopillars located at the HTL/EML interface.

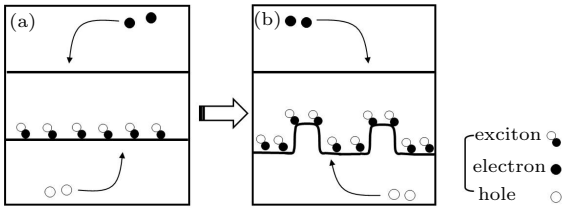


Fig. 8. The illustration of the carrier injection and recombination for (a) the reference device and (b) the device with a nanopillar pattern at the HTL/EML interface.

4. Conclusions

In this study, we have introduced a nanopillar pattering structure at the ETL/cathode and HTL/EML interfaces to improve the efficiency of OLEDs. By optimizing the number, height, and position of the nanopillars, we find that the device with two nanopillars and an optimized nanopillar thickness of 15 nm at the HTL/EML interface layer exhibits the best current efficiency of 27.05 cd/A and power efficiency of 13.06 lm/w, which are 1.78 and 2.47 times that of the reference device. Therefore, it is concluded that the nanopillar patterning structure in the device can effectively increase the carrier injection, broaden the carrier recombination zone, and improve light extraction into an external mode.

References

[1] Sun Y, Giebink N C, Kanno H, Ma B, Thompson M E and Forrest S R 2006 *Nature* **440** 908
[2] Li J F, Hu L B, Wang L, Zhou Y X, Gruner G and Marks T J 2006 *Nano Lett.* **6** 2472
[3] Segal M, Singh M, Rivoire K, Difley S, Voorhis T V and Baldo M A 2007 *Nat. Mater.* **6** 374
[4] Sun Y and Forrest S R 2008 *Nat. Photon.* **2** 483
[5] Reineke S, Lindner F, Schwartz G, Seidler N, Walzer K, Lüssem B and Leo K 2009 *Nature* **459** 234
[6] Yu J N, Lin H, Wang F F, Lin Y, Zhang J H, Zhang H, Wang Z X and Wei B 2012 *J. Mater. Chem.* **22** 22097
[7] Wei B, Liu J Z, Zhang Y, Zhang J H, Peng H N, Fan H L, He Y B and Gao X C 2010 *Adv. Funct. Mater.* **20** 2448
[8] Patel N, Cina K S J and Burroughes H 2002 *IEEE J. Sel. Top. Quantum Electron.* **8** 346
[9] Meerholz K and Muller D C 2001 *Adv. Funct. Mater.* **11** 251
[10] Tsutsui T, Aminaka E, Lin C P and Kim D U 1997 *Philos. Trans. R. Soc. London Ser. A* **355** 801
[11] Yu J N, Zhang M Y, Li C, Shang Y Z, Lü Y F, Wei B and Huang W 2012 *Chin. Phys. B* **21** 083303
[12] Cao J S, Guan M, Cao G H, Zeng Y P, Li J M and Qin D S 2008 *Chin. Phys. B* **17** 2725
[13] Matterson B J, Lupton J M, Safonov A F, Salt M G, Barnes W L and Samuel I D W 2001 *Adv. Mater.* **13** 123
[14] Riel H, Karg S, Beierlin T, Ruhstaller B and Rieb W 2003 *Appl. Phys. Lett.* **82** 466
[15] Lee Y J, Kim S H, Huh J, Kim G H, Lee Y H, Cho S H, Kim Y C and Do Y R 2003 *Appl. Phys. Lett.* **82** 3779
[16] Joannopoulos J D, Villeneuve P R and Fan S 1997 *Nature* **386** 143
[17] Shao M, Guo X, Chen S F, Fan Q L and Huang W 2012 *Chin. Phys. B* **21** 108507
[18] Boroditsky M, Krauss T F, Coccioli R, Vrijen R, Bhat R and Yablonovitch E 1999 *Appl. Phys. Lett.* **75** 1036
[19] Ryu H Y, Lee Y H, Sellin R L and Bimberg D 2001 *Appl. Phys. Lett.* **79** 3573
[20] Papadimitrakopoulos F, Zang X M, Thomsen D L and Higginson K A 1996 *Chem. Mater.* **8** 1363
[21] Fukuda T, Wei B, Fujimaki M, Ichikawa M, Koyama T and Taniguchi Y 2007 *Jpn. J. Appl. Phys.* **46** 642
[22] Adawi A M, Kullock R, Rurner J L, Vasilev C, Lidzey D G, Tahraoui A, Fry PW, Gibson D, Smith E, Foden C, Roberts M, Qureshi F and Athanassopoulou N 2006 *Org. Electron.* **7** 222
[23] Do Y R, Kim Y C, Song Y W, Cho C O, Jeon H, Lee Y J, Kim S H and Lee Y H 2003 *Adv. Mater.* **15** 1214
[24] Ho Y H, Liu C C, Liu S W, Liang H, Chu C W and Wei P K 2011 *Opt. Express* **19** A295
[25] Chutinan A, Ishihara K, Asano T, Fujita M and Noda S 2005 *Org. Electron.* **6** 3
[26] Nakamura T, Tsutsumi N, Juni N and Fujii H 2005 *J. Appl. Phys.* **97** 054505